


Mechanistic Understanding of Oxygen Activation on Bulk Au(111) Surface Using Tip-Enhanced Raman Spectroscopy

Journal Article

Author(s):

Cai, Zhen-Feng; Tang, Zi-Xi; Zhang, Yao; [Kumar, Naresh](#) 

Publication date:

2024

Permanent link:

<https://doi.org/10.3929/ethz-b-000667315>

Rights / license:

[Creative Commons Attribution-NonCommercial-NoDerivatives 4.0 International](#)

Originally published in:

Angewandte Chemie. International Edition, <https://doi.org/10.1002/anie.202318682>

Funding acknowledgement:

741431 - Nanoscale Vibrational Spectroscopy of Sensitive 2D Molecular Materials (EC)

Oxygen Activation

Mechanistic Understanding of Oxygen Activation on Bulk Au(111) Surface Using Tip-Enhanced Raman Spectroscopy

Zhen-Feng Cai,* Zi-Xi Tang, Yao Zhang, and Naresh Kumar*

Abstract: Gaining mechanistic understanding of oxygen activation on metal surfaces is a topical area of research in surface science. However, direct investigation of on-surface oxidation processes at the nanoscale and the empirical validation of oxygen activation pathways remain challenging for the conventional analytical tools. In this study, we applied tip-enhanced Raman spectroscopy (TERS) to gain mechanistic insights into oxygen activation on bulk Au(111) surface. Specifically, oxidation of 4-aminothiophenol (4-ATP) to 4-nitrothiophenol (4-NTP) on Au(111) surface was investigated using hyperspectral TERS imaging. Nanoscale TERS images revealed a markedly higher oxidation efficiency in disordered 4-ATP adlayers compared to the ordered adlayers signifying that the oxidation of 4-ATP molecules proceeds via interaction with the on-surface oxidative species. These results were further validated via direct oxidation of the 4-ATP adlayers with H₂O₂ solution. Finally, TERS measurements of oxidized 4-ATP adlayers in the presence of H₂O¹⁸ provided the first empirical evidence for the generation of oxidative species on bulk Au(111) surface via water-mediated activation of molecular oxygen. This study expands our mechanistic understanding of oxidation chemistry on bulk Au surface by elucidating the oxygen activation pathway.

The activation of molecular oxygen on metal surfaces has been a topic of great interest in the field of surface science.^[1–5] Understanding the oxygen activation mechanism is crucial for the development of efficient catalysts for oxidative chemical reactions. Oxygen activation is known to be promoted by photons,^[6,7] metal surfaces,^[1,8] surface plasmon resonance^[9,10] and hydrogen.^[11,12] Additionally, on small (<2 nm) Au nanoparticles supported on TiO₂, Al₂O₃ or SiO₂, water/moisture is known to play a significant role in several oxygen-involved reactions including CO oxidation,^[13,14] propene epoxidation,^[15,16] and alcohol oxidation.^[17] Although small Au nanoparticles have shown promising catalytic activity for oxidation reactions, this hasn't been the case for bulk Au(111) surface. However, some theoretical studies using density functional theory (DFT) have indicated that on bulk Au(111) surface, adsorption energy of molecular oxygen can be significantly increased in the presence of water and oxidative species can be generated from a H₂O–O₂ complex.^[18,19] But the limited sensitivity and spatial resolution of the conventional analytical tools make it very challenging to directly probe the on-surface oxidation processes and obtain empirical evidence for the water-promoted oxygen activation pathway on the bulk Au(111) surface. To the best of our knowledge, other than theoretical investigations, the water-promoted activation of molecular oxygen on bulk Au(111) surface has not been experimentally proven so far.

In the last two decades, tip-enhanced Raman spectroscopy (TERS) has emerged as a powerful tool for investigating chemical reactions at molecular level.^[20–23] In TERS, laser irradiation at the apex of a metallic tip generates a highly localized and enhanced electromagnetic field (also called near-field) in the tip-sample junction via a combination of localized surface plasmon resonance and lightning rod effect.^[24–27] This near-field can be applied to probe surface molecular transformations with a high sensitivity and nanoscale resolution. In this manner, TERS combines the high spatial resolution of scanning probe microscopy with the chemical specificity and sensitivity of surface-enhanced Raman spectroscopy.^[28–30] TERS has been successfully used to study a wide range of chemical reactions on surfaces, including catalytic coupling,^[31,32] decomposition,^[33–35] polymerization,^[36,37] and hydrogenation^[38] reactions offering valuable insights into the reaction intermediates and pathways.

In this work, we have successfully applied TERS to gain mechanistic insights in oxygen activation on bulk Au(111) surface for the first time. To this end, self-assembled

[*] Dr. Z.-F. Cai

Key Laboratory of Green Chemistry and Technology of Ministry of Education, College of Chemistry, Sichuan University
 29 Wangjiang Road, Chengdu 610064 (P. R. China)
 E-mail: caizf@scu.edu.cn

Dr. Z.-F. Cai, Dr. N. Kumar

Department of Chemistry and Applied Biosciences, ETH Zurich
 Vladimir-Prelog-Weg 3, Zurich CH-8093 (Switzerland)
 E-mail: naresh.kumar@org.chem.ethz.ch

Z.-X. Tang, Prof. Y. Zhang

Hefei National Laboratory for Physical Sciences at the Microscale and Synergetic Innovation Center of Quantum Information and Quantum Physics, University of Science and Technology of China, 230026 Hefei, Anhui, (P. R. China)

© 2024 The Authors. Angewandte Chemie International Edition published by Wiley-VCH GmbH. This is an open access article under the terms of the Creative Commons Attribution Non-Commercial NoDerivs License, which permits use and distribution in any medium, provided the original work is properly cited, the use is non-commercial and no modifications or adaptations are made.

monolayer (SAM) of organic molecules offer an effective model system to gain mechanistic insights into on-surface oxidative processes.^[39,40] Herein, we applied TERS to investigate oxidation of 4-aminothiophenol (4-ATP) SAMs into 4-nitrothiophenol (4-NTP) on Au(111) surface. Hyper-spectral TERS imaging of 4-ATP adlayers on Au(111) exposed to O₂ showed a clear difference in the oxidation efficiency between samples with ordered and disordered molecular arrangements signifying that the oxidation of 4-ATP to 4-NTP occurs via interaction with on-surface oxidative species. Furthermore, oxidation using H₂O₂ solution showed a similar reaction efficiency in both ordered and disordered 4-ATP adlayers on Au(111) further substantiating the involvement of on-surface oxidative species in 4-ATP oxidation via O₂ exposure. Finally, controlled oxidation using H₂O¹⁸ provided direct evidence of molecular oxygen activation via water-promoted mechanism on bulk Au(111) surface for the first time. This fundamental work expands our mechanistic understanding of oxidation reactions on bulk Au surface by elucidating the role of water in O₂ activation.

Figure 1 illustrates the scanning tunneling microscopy (STM)-TERS setup used in this study to investigate the oxidation of 4-ATP on Au(111) surface. SAMs of 4-ATP molecules on atomically flat Au(111) surfaces (Figure S1) were prepared via two different methods: By overnight (12 hours) immersion of the Au(111) substrate in 4-ATP solution (Method I), and by treating the Au(111) substrate with a single drop of 4-ATP solution for less than 60 s (Method II). It is well known that the molecular arrangement of thiolate molecules on a metal surface critically depends on the self-assembly time.^[41,42] Long-term (several hours) immersion of a metal substrate in thiol solution typically leads to the formation of a SAM with a well-ordered (close-packed) molecular arrangement. Conversely, a short-term (few seconds) exposure of a metal substrate to thiol solution results in a SAM with a disordered molecular arrangement. We demonstrated this in our previous work,

where 12 hours immersion of the Au(111) substrate in a thiol solution generated a SAM with 74 % of the surface covered with well-ordered molecular domains, which was reduced to only 8 % when the metal substrate was exposed to the thiol solution for less than 60 s.^[31] For ease of discussion, we will refer to the samples prepared by Methods I and II as the ordered and disordered samples, respectively.

We first investigated if the 4-ATP molecules on bulk Au(111) surface can indeed be oxidized to 4-NTP by exposure to O₂. Figure 2a displays the averaged TERS spectra of the 4-ATP adlayers on the disordered sample after 0, 10, 60, and 300 minutes of O₂ exposure. Reference Raman spectra of bulk 4-ATP (Ref_{4-ATP}) and 4-NTP (Ref_{4-NTP}) are also plotted for comparison. In comparison to the Raman spectrum of bulk 4-ATP, four new bands at 1146, 1335, 1390, and 1442 cm⁻¹ (highlighted with red and blue stripes) are observed in the TERS spectra of the 4-ATP adlayer after O₂ treatments. Based on the theoretical and experimental reports in literature,^[43,44] these new Raman bands are assigned to the C–H bending (1146 cm⁻¹) and N=N stretching (1390 and 1442 cm⁻¹) modes of p,p'-dimercaptoazobenzene (DMAB)^[45] and the NO₂ (1335 cm⁻¹) stretching mode of 4-NTP.^[31] This confirms that after O₂ exposure the 4-ATP molecules on bulk Au(111) surface are transformed into two competing products: (1) 4-NTP via oxidation and (2) DMAB via plasmon-driven photocatalytic dimerization. Interestingly, the competing oxidation and photocatalytic dimerization reactions display opposite trends with the increasing O₂ exposure. As the O₂ treatment time increases from 0 to 300 minutes, intensity of the 4-NTP signal at 1335 cm⁻¹ (red stripe) steadily increases indicating a progressively higher amount of 4-NTP formation. This trend is more clearly visible in Figure 2b, where intensity ratio of the 4-NTP signal at 1335 cm⁻¹ and 4-ATP signal at 1080 cm⁻¹ (I_{1335}/I_{1080}) show an increasing trend with longer O₂ exposure time. Furthermore, in Figure 2a, steady broadening of the C–C stretching mode of 4-ATP at 1589 cm⁻¹ with prolonged O₂ exposure due to the appear-

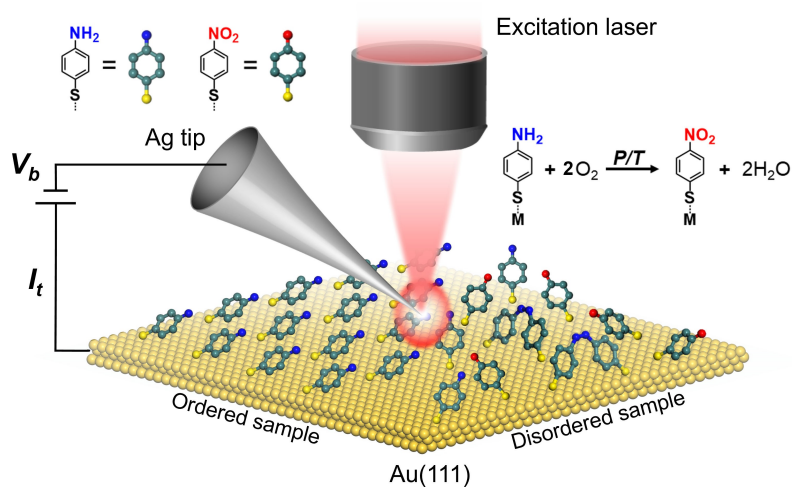


Figure 1. Schematic diagram of the STM-TERS setup used in this study to investigate the on-surface oxidation of ordered and disordered 4-ATP adlayers on Au(111) surface.

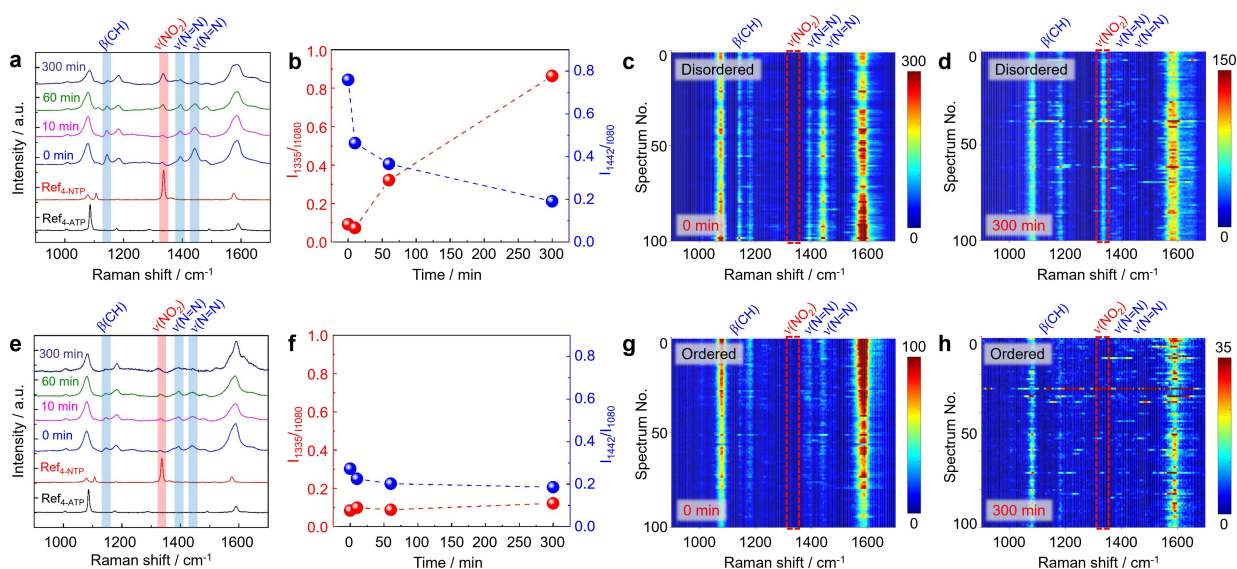


Figure 2. Average TERS spectra showing time-dependent oxidation of 4-ATP adlayer on the (a) disordered and (e) ordered 4-ATP/Au(111) samples. Each spectrum represents an average of 100 TERS spectra measured in a TERS image of $1 \mu\text{m}^2$ with a step size of 100 nm. Raman spectra of bulk 4-NTP and 4-ATP are also plotted for comparison. (b,f) Plots of the TERS intensity ratio of 1335 cm^{-1} and 1080 cm^{-1} signals (I_{1335}/I_{1080}) and 1442 cm^{-1} and 1335 cm^{-1} signals (I_{1442}/I_{1335}) as a function of O_2 exposure time observed in the TERS measurements presented in Panels a and e. Waterfall plots of 100 spectra measured in the TERS images of 4-ATP adlayers on the (c,d) disordered and (g,h) ordered samples with O_2 exposure times of 0 and 300 minutes.

ance of C–C stretching mode of 4-NTP at 1575 cm^{-1} also supports this trend. On the other hand, the intensity of the DMAB signals (blue stripes) exhibit a gradual reduction with prolonged exposure to O_2 in Figure 2a. This is also evident in Figure 2b, where intensity ratio of the DMAB signal at 1442 cm^{-1} and the 4-ATP signal at 1080 cm^{-1} (I_{1442}/I_{1080}) show a decreasing trend with longer O_2 exposure time.

To confirm if these spectral changes occur over the entire Au(111) surface, 100 spectra measured in the TERS images of the disordered sample after O_2 treatment times of 0, 60, and 300 minutes are presented as waterfall plots in Figures 2c, S2a and 2d, respectively. These plots clearly display a steady increase in the intensity of 4-NTP signal at 1335 cm^{-1} and a steady decrease in the intensity of DMAB signals at 1146, 1390, and 1442 cm^{-1} with prolonged O_2 exposure time. These findings signify that as the number of oxidized 4-NTP molecules in the 4-ATP adlayer increases, the photocatalytic dimerization of 4-ATP molecules into DMAB decreases due to the progressive reduction in the number of adjacent 4-ATP molecules needed for dimerization.

Notably, in the case of ordered 4-ATP/Au(111) sample, a significantly lower intensity of the 4-NTP and DMAB signals is observed in the TERS spectra, which doesn't change significantly with increasing O_2 exposure as shown in the averaged TERS spectra in Figure 2e, ratio plots in Figure 2f, and the waterfall plots in Figures 2g, S2b, and 2h. Note that the variation in the intensity of $\nu(\text{NO}_2)$ and $\nu(\text{N=N})$ signals in Figures 2a and 2e represent different amounts of 4-NTP and DMAB molecules as Raman signal is directly proportional to the number of molecules. This indicates that 4-ATP molecules within the close-packed

SAM of the ordered sample are considerably more resistant to oxidation into 4-NTP as well as photocatalytic dimerization into DMAB.^[38,44]

The significant difference in the oxidation level of 4-ATP adlayers in the disordered and ordered samples indicates that the oxidation of the 4-ATP molecules occurs via interaction with the oxidative species generated on Au(111) surface. It has been previously shown that the thiolate molecules adsorbed on a metal can transiently tilt down and interact with the surface reactive species.^[38] Whilst in the rigid close-packed structure of the ordered sample it is difficult for the 4-ATP molecules to bend towards the Au(111) substrate, this can be easily accomplished in the disordered sample where 4-ATP molecules can flexibly bend towards the Au(111) substrate and interact with the on-surface oxidative species resulting in a higher oxidation level.

To spatially visualize the on-surface oxidation at the nanoscale, we performed high-resolution hyperspectral TERS imaging (with 3.3 nm step size) of the ordered and disordered 4-ATP/Au(111) samples after 5 hours of O_2 treatment. Figure 3a showcases TERS image of the 1335 cm^{-1} signal measured on the ordered sample post- O_2 exposure. Interestingly, a very weak 1335 cm^{-1} signal is observed across the sample surface indicating a very low level of 4-ATP oxidation into 4-NTP. Six representative TERS spectra from the surface sites labeled in Figure 3a are presented in Figure 3b. Notably, 87% of the surface sites like P1, P2, and P3, displayed a complete absence of the 4-NTP signal whilst 4-NTP formation was apparent only in a few isolated sites like P4, P5, and P6 (Figure 3b). Schematic

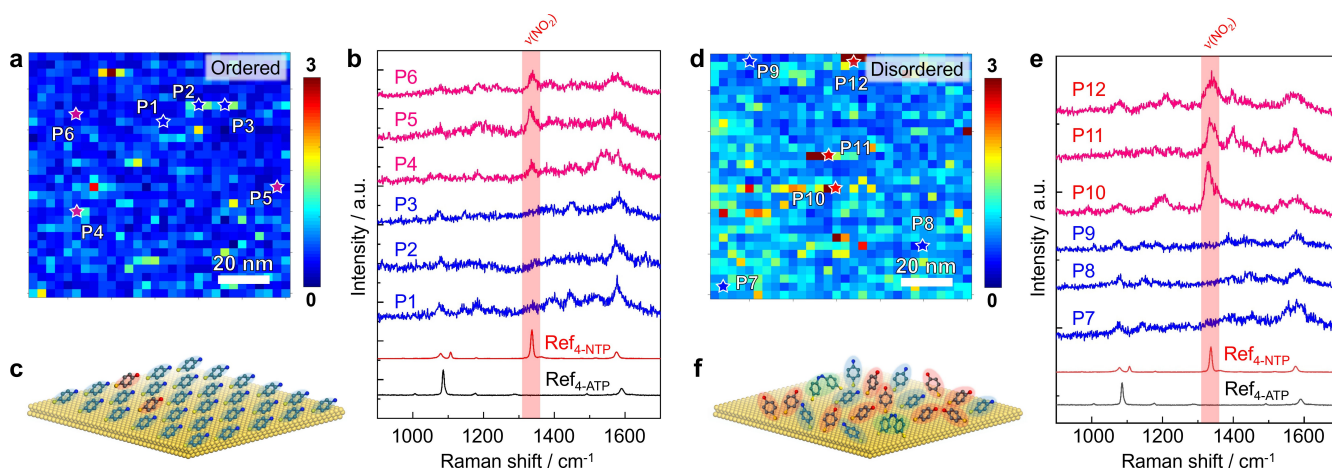


Figure 3. TERS images of the 1335 cm^{-1} signal measured on the 4-ATP adlayers on the (a) ordered and (d) disordered samples after 5 hours of O_2 treatment. Step size: 3.3 nm . Spectrum integration time: 1 s . (b,e) TERS spectra measured at the sites P1–P12 marked in Panels a and d. Schematic illustration of the 4-ATP adlayers on the (c) ordered and (f) disordered samples post-oxidation.

illustration of the post-oxidation 4-ATP adlayer on the ordered sample is presented in Figure 3c.

On the other hand, the disordered sample displayed a markedly higher 1335 cm^{-1} signal across the entire sample surface (Figure 3d) indicating a significantly higher level of 4-ATP oxidation. Figure 3e showcases six example TERS spectra from different surface sites. Notably, 54% of the surface sites like P10, P11, and P12 exhibited a pronounced 4-NTP signal whilst Raman signature of the unreacted 4-ATP was discernible only at a few sites like P7, P8, and P9. Schematic illustration of the post-oxidation 4-ATP adlayer on the disordered sample is presented in Figure 3f. The STM images measured simultaneously with the TERS images in Figures 3a and 3d are presented in Figures S3, where a relatively higher roughness is observed on the disordered sample confirming a relatively higher molecular

disorder. The relatively higher oxidation efficiency across the disordered 4-ATP adlayer evident through the nanoscale TERS imaging further confirms that the formation of 4-NTP occurs via interaction of 4-ATP molecules with the oxidative species formed on the Au(111) surface.

We next investigated the oxidation of the disordered and ordered 4-ATP adlayers via H_2O_2 treatment. Average TERS spectra presented in Figures 4a and 4b display the time-dependent oxidation of 4-ATP adlayers on the ordered and disordered samples after immersion in H_2O_2 solution for 0, 1, 2, and 4 minutes. Waterfall plots of the spectra measured in the corresponding TERS images are presented in Figure S4. In Figures 4a and 4b, a clear 4-NTP signal at 1335 cm^{-1} with a similar intensity is observed in the TERS spectra of both disordered and ordered samples signifying comparable oxidation of 4-ATP to 4-NTP. This is further

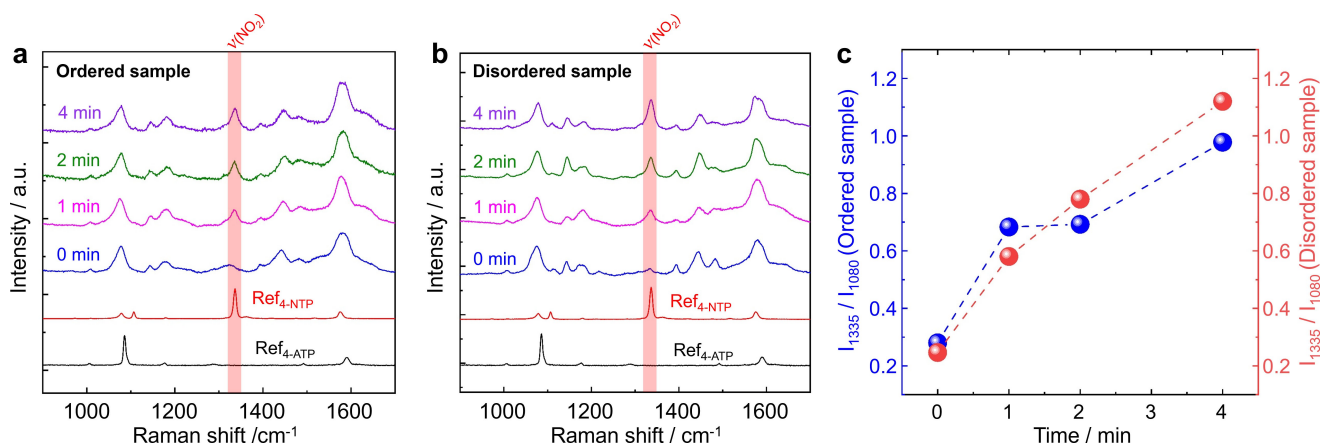


Figure 4. Average TERS spectra showing the time-dependent oxidation of 4-ATP adlayers on the (a) ordered and (b) disordered samples after 0, 1, 2, and 4 minutes of H_2O_2 treatment. Each spectrum represents an average of 100 TERS spectra measured in a TERS image of $1\text{ }\mu\text{m}^2$ with a step size of 100 nm . Reference Raman spectra of the bulk 4-NTP and 4-ATP are also plotted for comparison. (c) Plots of the TERS intensity ratio of 1335 cm^{-1} and 1080 cm^{-1} signals (I_{1335}/I_{1080}) as a function of H_2O_2 treatment time observed in the TERS measurements presented in Panels a and b.

evident in Figure 4c where the 1335 cm^{-1} signal measured on the ordered and disordered samples is plotted against the H_2O_2 treatment time. Both samples show a similar level of 4-NTP formation after equal amounts of H_2O_2 treatment.

In H_2O_2 solution, the abundant oxidative species are able to directly interact with the amine moiety of 4-ATP molecules in the ordered and disordered samples. This eliminates the necessity for 4-ATP molecules to bend towards the Au(111) surface to engage with oxidative species like in the case of O_2 treatment (Figures 2 and 3), which results in a comparable oxidation efficiency on both samples. This suggests that in the TERS measurements of the ordered and disordered samples after O_2 exposure presented in Figures 2 and 3, O_2 molecules do not directly interact with and oxidize the $-\text{NH}_2$ moiety of 4-ATP molecules. Rather, the O_2 molecules form oxidative species on the Au(111) surface and then interact with the 4-ATP molecules in the ordered and disordered adlayers in a dissimilar fashion due to steric hindrance resulting in a dramatically different oxidation efficiency.

A key question that arises from the TERS measurements of 4-ATP adlayers after O_2 exposure (Figures 2 and 3) is: How can the 4-ATP molecules oxidize to 4-NTP considering the direct activation of O_2 on the Au(111) surface is a very

difficult process (activation barrier of $2.44\text{ eV}^{[1]}$)? It is known that under ambient conditions, an interfacial water layer is present on Au(111) surface due to the relative humidity.^[46–48] Theoretical studies have proposed that water molecules present on an atomically flat bulk Au(111) surface can interact with molecular oxygen to form a $\text{H}_2\text{O}-\text{O}_2$ complex, which can heterolytically cleave to produce oxidative hydroperoxyl, atomic oxygen, and hydroxyl species as schematically illustrated in Figure 5a.^[18] These oxidative species can oxidize 4-ATP molecules to 4-NTP. However, the water-promoted oxygen activation on bulk Au(111) surface has not been experimentally proven so far. To verify this hypothesis, we performed a TERS experiment by adding $5\text{ }\mu\text{L H}_2\text{O}^{18}$ to the surface of disordered 4-ATP/Au(111) sample prior to 5 hours of O_2 exposure. Figure 5b shows the waterfall plot of 100 TERS spectra measured from the H_2O^{18} -treated 4-ATP adlayer, where a clear 4-NTP signal confirms the oxidation of 4-ATP molecules. Figure 5c displays a comparison of the average spectra measured in the TERS images of 4-ATP/Au(111) samples with and without H_2O^{18} treatment. A clear 4-NTP signal is visible in the TERS spectra of both samples. An expanded view of the $1320\text{--}1347\text{ cm}^{-1}$ region of the TERS spectra is plotted in Figure 5d. Notably, the position of the $\nu(\text{NO}_2)$ signal of 4-

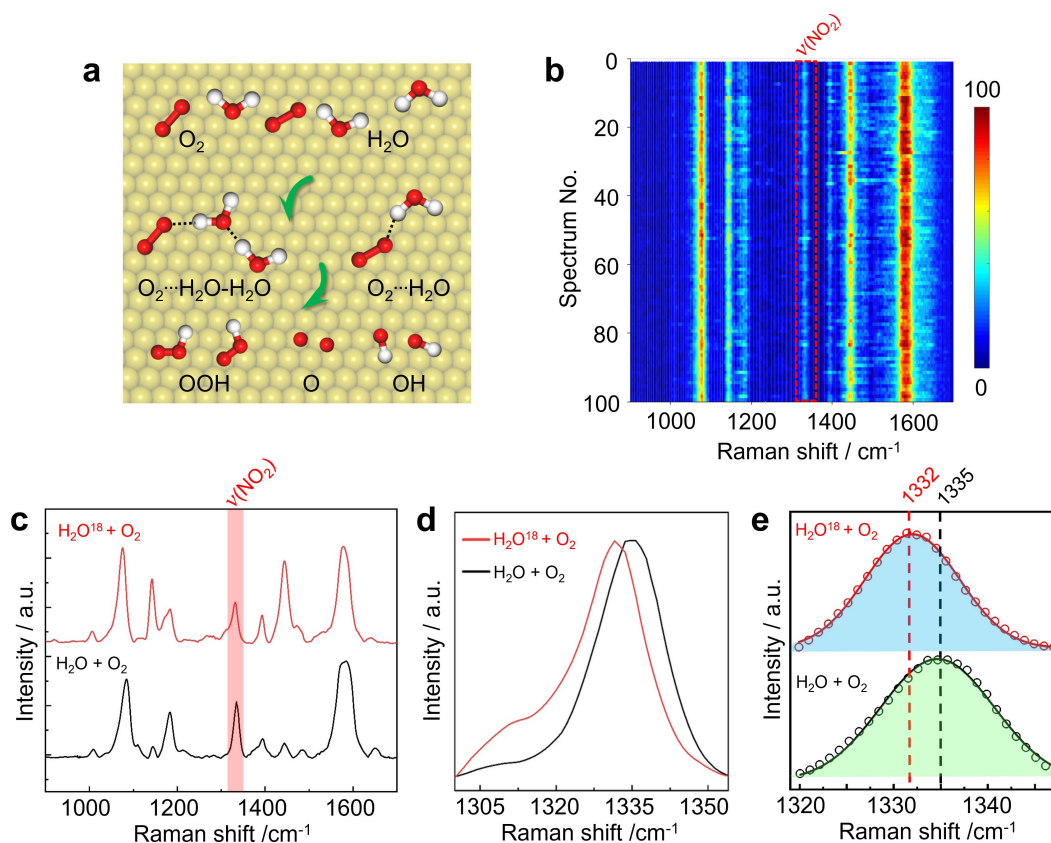


Figure 5. (a) Schematic diagram illustrating the theoretically proposed water-promoted mechanism of O_2 activation on Au(111) surface.^[18] (b) Waterfall plot of 100 TERS spectra measured in a $1\text{ }\mu\text{m}^2$ TERS image with a step size of 100 nm on a H_2O^{18} -treated disordered 4-ATP/Au(111) sample after 5 hours of O_2 exposure. (c) Comparison of the average TERS spectra measured in the TERS images of disordered 4-ATP/Au(111) samples with (red trace) and without (black trace) H_2O^{18} treatment after 5 hours of O_2 exposure. (d) Expanded view of the normalized $1320\text{--}1347\text{ cm}^{-1}$ region highlighted by red stripe in Panel c. (e) Gaussian fitting of the average TERS spectra shows that the spectral position of the $\nu(\text{NO}_2)$ signal in the TERS spectra of H_2O^{18} -treated 4-ATP adlayer is red-shifted by 3 cm^{-1} compared to the 4-ATP adlayer without H_2O^{18} treatment.

NTP shows a clear red-shifted in the TERS spectrum of the H_2O^{18} -treated 4-ATP adlayer. Using Gaussian fitting of the TERS spectra in Figure 5e, the red-shift is estimated to be 3 cm^{-1} . In addition to the isotopic shifts (Figure 5c), a relatively higher intensity of DMAB signals at 1120 and 1430 cm^{-1} is observed in the H_2O^{18} -treated 4-ATP adlayer presumably due to the higher molecular disorder induced by the H_2O^{18} treatment.^[31]

10 spectra from across the TERS image of H_2O^{18} -treated 4-ATP adlayer are presented in Figure S5. In all these spectra, the position of the 4-NTP signal is red-shifted compared to the 4-ATP adlayer without H_2O^{18} treatment showing that this effect is observed all across the sample surface. Interestingly, a variable red-shift of the $\nu(\text{NO}_2)$ signal is observed in the TERS spectra across the sample as shown in Figure S6. A detailed analysis and discussion is presented in the caption of Figure S6.

It is well known that the increased mass of a heavier isotope induces red-shift in the energy of a Raman vibrational mode.^[49] To demonstrate this, we performed DFT simulations of the Raman spectra of 4-NTP molecules with 0 - 2 O^{18} atoms in the $-\text{NO}_2$ moiety, which are presented in Figure S7. DFT calculations show that in 4-NTP molecules with one and two O^{18} atoms in the $-\text{NO}_2$ moiety, the $\nu(\text{NO}_2)$ vibrational mode is red-shifted. Therefore, red-shift of the $\nu(\text{NO}_2)$ signal in our experimental TERS spectra confirms incorporation of O^{18} into the $-\text{NO}_2$ moiety of 4-NTP molecules. Furthermore, as expected, the 4-NTP molecule with two O^{18} atoms shows a larger red-shift compared to the 4-NTP molecule with one O^{18} atom. However, based on the spatially variable red-shift of $\nu(\text{NO}_2)$ signal observed in the TERS measurements (Figure S6), it is not possible to determine with certainty if one or both oxygen atoms incorporated in the $-\text{NO}_2$ moiety of 4-NTP molecules are O^{18} . Nevertheless, the experimental TERS spectra and DFT calculations strongly indicate that on bulk Au(111) surface, the oxidative species involved in the oxidation of 4-ATP molecules to 4-NTP are indeed generated via interaction of molecular oxygen with water. These results constitute the first direct empirical evidence of the water-promoted activation mechanism of O_2 on Au(111) surface. Further investigation of the nature of $\text{H}_2\text{O}-\text{O}_2$ complex is underway in our laboratory.

In summary, herein we applied hyperspectral TERS imaging to investigate the oxidation of 4-ATP adlayers on Au(111) surface, to obtain mechanistic insights pertaining to the structure–reactivity relationships and oxygen activation pathways. Our findings shed light on several aspects of the on-surface oxidation process. For instance, the nanoscale resolution TERS imaging of oxidized samples revealed a higher reaction efficiency in the disordered sample as compared to the ordered sample. These results demonstrated that the oxidation of 4-ATP molecules proceeds via interaction with on-surface oxidative species. This was further validated via direct oxidation of 4-ATP adlayers in H_2O_2 solution, where in the absence of the molecular bending requirement, a similar oxidation efficiency was observed on both ordered and disordered samples. Finally, oxidation of 4-ATP molecules in the presence of H_2O^{18}

provided the first empirical evidence for the generation of active oxidative species on Au(111) surface through a water-promoted O_2 activation mechanism. This insight has significant implications, as it elucidates the molecular oxygen activation pathway on bulk Au surface. By bridging the gap between theory and experimentation, this study deepens our fundamental understanding of on-surface oxidation chemistry on Au.

Supporting Information

The authors have cited additional references within the Supporting Information.

Acknowledgements

The authors acknowledge funding from the ERC program (Grant No. 741431). ZFC acknowledges financial support from the Fundamental Research Funds for the Central Universities. Open Access funding provided by Eidgenössische Technische Hochschule Zürich.

Conflict of Interest

The authors declare no conflict of interest.

Data Availability Statement

The data that support the findings of this study are openly available in ETH Zurich Research Collection at <https://doi.org/10.3929/ethz-b-000645782>.

Keywords: Oxidation · Oxygen Activation · Surface Chemistry · Nanoimaging · Tip-Enhanced Raman Spectroscopy

- [1] M. M. Montemore, M. A. van Spronsen, R. J. Madix, C. M. Friend, *Chem. Rev.* **2018**, *118*, 2816–2862.
- [2] A. Staykov, H. Tellez, T. Akbay, J. Druce, T. Ishihara, J. Kilner, *Chem. Mater.* **2015**, *27*, 8273–8281.
- [3] D. Widmann, R. J. Behm, *Acc. Chem. Res.* **2014**, *47*, 740–749.
- [4] K. Zhao, L. Z. Zhang, J. J. Wang, Q. X. Li, W. W. He, J. J. Yin, *J. Am. Chem. Soc.* **2013**, *135*, 15750–15753.
- [5] R. Long, K. K. Mao, X. D. Ye, W. S. Yan, Y. B. Huang, J. Y. Wang, Y. Fu, X. S. Wang, X. J. Wu, Y. Xie, Y. J. Xiong, *J. Am. Chem. Soc.* **2013**, *135*, 3200–3207.
- [6] B. S. Li, S. Y. Liu, C. Lai, G. M. Zeng, M. M. Zhang, M. Z. Zhou, D. L. Huang, L. Qin, X. G. Liu, Z. W. Li, N. An, F. H. Xu, H. Yi, Y. J. Zhang, L. Chen, *Appl. Catal. B* **2020**, *266*, 1118650.
- [7] Y. Yang, C. Zhang, D. L. Huang, G. M. Zeng, J. H. Huang, C. Lai, C. Y. Zhou, W. J. Wang, H. Guo, W. J. Xue, R. Deng, M. Cheng, W. P. Xiong, *Appl. Catal. B* **2019**, *245*, 87–99.
- [8] W.-L. Yim, T. Klüner, *J. Catal.* **2008**, *254*, 349–354.
- [9] Y. X. Li, M. M. Wen, Y. Wang, G. Tian, C. Y. Wang, J. C. Zhao, *Angew. Chem. Int. Ed.* **2021**, *60*, 910–916.

- [10] Y.-F. Huang, M. Zhang, L.-B. Zhao, J.-M. Feng, D.-Y. Wu, B. Ren, Z.-Q. Tian, *Angew. Chem. Int. Ed.* **2014**, *53*, 2353–2357.
- [11] S. M. Lang, T. M. Bernhardt, R. N. Barnett, B. Yoon, U. Landman, *J. Am. Chem. Soc.* **2009**, *131*, 8939–8951.
- [12] R. Zhang, T. Ran, Y. Cao, Q. Zhang, F. Dong, G. Yang, Y. Zhou, *Environ. Sci. Technol.* **2020**, *54*, 16221–16230.
- [13] M. Daté, M. Okumura, S. Tsubota, M. Haruta, *Angew. Chem. Int. Ed.* **2004**, *43*, 2129–2132.
- [14] H. H. Kung, M. C. Kung, C. K. Costello, *J. Catal.* **2003**, *216*, 425–432.
- [15] S. Lee, L. M. Molina, M. J. López, J. A. Alonso, B. Hammer, B. Lee, S. Seifert, R. E. Winans, J. W. Elam, M. J. Pellin, S. Vajda, *Angew. Chem. Int. Ed.* **2009**, *48*, 1467–1471.
- [16] J. Huang, T. Akita, J. Faye, T. Fujitani, T. Takei, M. Haruta, *Angew. Chem. Int. Ed.* **2009**, *48*, 7862–7866.
- [17] X. Yang, X. Wang, C. Liang, W. Su, C. Wang, Z. Feng, C. Li, J. Qiu, *Catal. Commun.* **2008**, *9*, 2278–2281.
- [18] C.-R. Chang, X.-F. Yang, B. Long, J. Li, *ACS Catal.* **2013**, *3*, 1693–1699.
- [19] M. Yan, Z.-Q. Huang, Y. Zhang, C.-R. Chang, *Phys. Chem. Chem. Phys.* **2017**, *19*, 2364–2371.
- [20] N. Kumar, B. M. Weckhuysen, A. J. Wain, A. J. Pollard, *Nat. Protoc.* **2019**, *14*, 1169–1193.
- [21] X. Wang, S.-C. Huang, S. Hu, S. Yan, B. Ren, *Nat. Rev. Phys.* **2020**, *2*, 253–271.
- [22] L. Li, J. F. Schultz, S. Mahapatra, X. Liu, C. Shaw, X. Zhang, M. C. Hersam, N. Jiang, *J. Am. Chem. Soc.* **2021**, *143*, 15624–15634.
- [23] S. Mahapatra, Y. Ning, J. F. Schultz, L. Li, J.-L. Zhang, N. Jiang, *Nano Lett.* **2019**, *19*, 3267–3272.
- [24] P. Verma, *Chem. Rev.* **2017**, *117*, 6447–6466.
- [25] W. Su, N. Kumar, A. Krayev, M. Chaigneau, *Nat. Commun.* **2018**, *9*, 2891.
- [26] T. Touzalin, S. Joiret, E. Maisonhaute, I. T. Lucas, *Anal. Chem.* **2017**, *89*, 8974–8980.
- [27] A. Weber-Bargioni, A. Schwartzberg, M. Cornaglia, A. Ismach, J. J. Urban, Y. Pang, R. Gordon, J. Bokor, M. B. Salmeron, D. F. Ogletree, P. Ashby, S. Cabrini, P. J. Schuck, *Nano Lett.* **2011**, *11*, 1201–1207.
- [28] Z.-F. Cai, N. Kumar, R. Zenobi, *CCS Chem.* **2023**, *5*, 55–71.
- [29] D. Mrdenović, Z.-F. Cai, Y. Pandey, G. L. Bartolomeo, R. Zenobi, N. Kumar, *Nanoscale* **2023**, *15*, 963–974.
- [30] A. B. Zrimsek, N. Chiang, M. Mattei, S. Zaleski, M. O. McAnally, C. T. Chapman, A.-I. Henry, G. C. Schatz, R. P. Van Duyne, *Chem. Rev.* **2017**, *117*, 7583–7613.
- [31] Z.-F. Cai, J. P. Merino, W. Fang, N. Kumar, J. O. Richardson, S. De Feyter, R. Zenobi, *J. Am. Chem. Soc.* **2022**, *144*, 538–546.
- [32] R. Wang, J. Li, J. Rigor, N. Large, P. Z. El-Khoury, A. Y. Rogachev, D. Kurouski, *J. Phys. Chem. C* **2020**, *124*, 2238–2244.
- [33] Z.-F. Cai, T. Käser, N. Kumar, R. Zenobi, *J. Phys. Chem. Lett.* **2022**, *13*, 4864–4870.
- [34] J. Xu, X. Zhu, S. Tan, Y. Zhang, B. Li, Y. Tian, H. Shan, X. Cui, A. Zhao, Z. Dong, J. Yang, Y. Luo, B. Wang, J. G. Hou, *Science* **2021**, *371*, 818–822.
- [35] J. Szczerbiński, J. B. Metternich, G. Goubert, R. Zenobi, *Small* **2020**, *16*, 1905197.
- [36] F. Shao, W. Wang, W. Yang, Z. Yang, Y. Zhang, J. Lan, A. D. Schlüter, R. Zenobi, *Nat. Commun.* **2021**, *12*, 4557.
- [37] F. Shao, W. Dai, Y. Zhang, W. Zhang, A. D. Schlüter, R. Zenobi, *ACS Nano* **2018**, *12*, 5021–5029.
- [38] H. Yin, L.-Q. Zheng, W. Fang, Y.-H. Lai, N. Porenta, G. Goubert, H. Zhang, H.-S. Su, B. Ren, J. O. Richardson, J.-F. Li, R. Zenobi, *Nat. Catal.* **2020**, *3*, 834–842.
- [39] H.-S. Su, H.-S. Feng, Q.-Q. Zhao, X.-G. Zhang, J.-J. Sun, Y. He, S.-C. Huang, T.-X. Huang, J.-H. Zhong, D.-Y. Wu, B. Ren, *J. Am. Chem. Soc.* **2020**, *142*, 1341–1347.
- [40] N. Kumar, B. Stephanidis, R. Zenobi, A. J. Wain, D. Roy, *Nanoscale* **2015**, *7*, 7133–7137.
- [41] S. Xu, S. J. N. Cruchon-Dupeyrat, J. C. Garno, G.-Y. Liu, G. K. Jennings, T.-H. Yong, P. E. Laibinis, *J. Chem. Phys.* **1998**, *108*, 5002–5012.
- [42] F. Schreiber, A. Eberhardt, T. Y. B. Leung, P. Schwartz, S. M. Wetterer, D. J. Lavrich, L. Berman, P. Fenter, P. Eisenberger, G. Scoles, *Phys. Rev. B* **1998**, *57*, 12476–12481.
- [43] Y.-F. Huang, H.-P. Zhu, G.-K. Liu, D.-Y. Wu, B. Ren, Z.-Q. Tian, *J. Am. Chem. Soc.* **2010**, *132*, 9244–9246.
- [44] H. Li, Z. X. Tang, J. X. Zhang, X. B. Zhang, Y. F. Zhang, Y. Zhang, Y. Zhang, Z. C. Dong, *Appl. Phys. A* **2023**, *129*, doi: 10.1007/s00339-00022-06263-00339.
- [45] N. Kumar, C. S. Wondergem, A. J. Wain, B. M. Weckhuysen, *J. Phys. Chem. Lett.* **2019**, *10*, 1669–1675.
- [46] Y. Pandey, D. F. Abbott, V. Mougél, N. Kumar, R. Zenobi, *Anal. Chem.* **2023**, *95*, 8869–8878.
- [47] J. Freund, J. Halbritter, J. K. H. Hörber, *Microsc. Res. Tech.* **1999**, *44*, 327–338.
- [48] N. Patel, M. C. Davies, M. Lomas, C. J. Roberts, S. J. B. Tendler, P. M. Williams, *J. Phys. Chem. B* **1997**, *101*, 5138–5142.
- [49] Z. Chen, D. W. Paley, L. Wei, A. L. Weisman, R. A. Friesner, C. Nuckolls, W. Min, *J. Am. Chem. Soc.* **2014**, *136*, 8027–8033.

Manuscript received: December 5, 2023

Accepted manuscript online: February 26, 2024

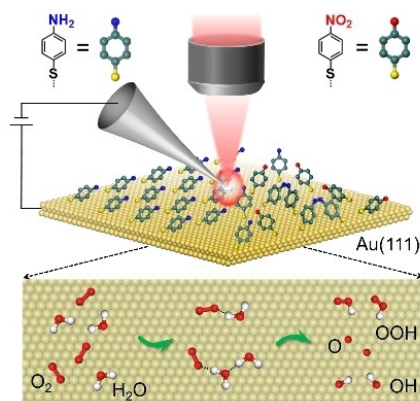
Version of record online: ■■■, ■■■

Communications

Oxygen Activation

Z.-F. Cai,* Z.-X. Tang, Y. Zhang,
N. Kumar* [e202318682](#)

Mechanistic Understanding of Oxygen Activation on Bulk Au(111) Surface Using Tip-Enhanced Raman Spectroscopy



Oxygen activation on bulk Au(111) surface is revealed for the first time using tip-enhanced Raman spectroscopy. Acti-

vation of molecular oxygen on bulk Au(111) surface is found to occur via a water-promoted mechanism.